International Journal of Computing and Digital Systems
ISSN (2210-142X)
Int. J. Com. Dig. Sys. #, No.# (Mon-20..)

Optimization of Equatorial Dipole-Dipole Antenna Geometry Using Evolutionary Computing for Subsurface Imaging

Ronnie Concepcion II[1,4,*], Jonah Jahara Baun[2,4], Adrian Genevie Janairo[2,4], Melchizedek Alipio[2,4], R-Jay Relano[1,4], Jason Española[1,4], Ryan Rhay Vicerra[1,4], Argel Bandala[2,4], Elmer Dadios[1,4], Jonathan Dungca[3,4]

[1] Department of Manufacturing Engineering and Management, De La Salle University, Manila, Philippines
[2] Department of Electronics and Computer Engineering, De La Salle University, Manila, Philippines
[3]Department of Civil Engineering, De La Salle University, Manila, Philippines
[4]Center for Engineering and Sustainability Development Research, De La Salle University, Manila, Philippines

E-mail address: ronnie.concepcion@dlsu.edu.ph, jonah_baun@dlsu.edu.ph, adrian_janairo@dlsu.edu.ph, melchizedek.alipio@dlsu.edu.ph, r-jay_relano@dlsu.edu.ph, jason.española@dlsu.edu.ph, ryan.vicerra@dlsu.edu.ph, argel.bandala@dlsu.edu.ph, elmer.dadios@dlsu.edu.ph, jonathan.dungca@dlsu.edu.ph

Received ## Mon. 20##, Revised ## Mon. 20##, Accepted ## Mon. 20##, Published ## Mon. 20##

Abstract: Efficient mapping of buried utilities requires vital subsurface imaging. However, traditional galvanic dipole antennas suffer from current leakage due to suboptimal geometry and necessitate destructive borehole methods. To address this, an evolutionary computing approach optimizes a single-pair equatorial dipole-dipole antenna for high-frequency capacitive ground coupling at 38 MHz with 1.2 m skin depth. By minimizing the induction number (β) to 0 and maximizing the electrostatic geometric factor (K) to 1, quasi-static condition is achieved. Multigene genetic programming constructs fitness functions using antenna geometry parameters: dipole spacing, dipole length, and plate elevation. The optimization utilizes a genetic algorithm (GA) and evolutionary strategy (ES) to find the optimal parameter combination. GA enables faster exploration, while ES facilitates faster exploitation. Results indicate that an optimized equatorial antenna design requires plate elevation to be $\leqslant$ 2.24% of the combined dipole spacing and length. The ES-optimized antenna exhibits minimal power loss, high efficiency, isotropic gain, and direct radiation of the electric field on the pipe surface. This study eliminates trial and error in dipole design by presenting an effective technique for antenna optimization in subsurface imaging. The proposed approach achieves the global best solution, improving the cost-effectiveness and efficiency of subsurface mapping.

Keywords: Antenna Geometry Optimization, Dipole Antenna, Machine Learning, Subsurface Imaging, Underground Imaging

1. INTRODUCTION

Subsurface imaging, otherwise known as geophysical imaging, utilizes electromagnetic signals in the lower spectrum to propagate high voltage, low current, and low power underground for certain purposes such as surveying buried artifacts, utilities, tunnels, presence of explosives, sinkholes, fresh water, and natural gas resources [1-4], monitoring of root zones that could affect industrial processes [5], and structural health monitoring [6-8]. The signal medium for subsurface imaging is different from conventional optical imaging as the latter uses high-powered cameras [9]. Geo-imaging is expected to penetrate signals through reinforced concretes and different types of soil [10]. It is dominantly dependent on the nature and geometry of the antenna and its corresponding transmitter and receiver subsystems and the target material [11]. The traditional approach of employing subsurface imaging is through a destructive borehole approach in which galvanic dipoles are inserted down the earth [12] and the use of laser emission for ultrasonic generation [13]. In the Philippines, there are very limited commercial geophysical service providers available that use advanced mapping technology such as the prominent ground penetrating radar (GPR), accelerographs, seismic refraction testing, and downhole

E-mail: ronnie.concepcion@dlsu.edu.ph, jonah_baun@dlsu.edu.ph, adrian_janairo@dlsu.edu.ph, melchizedek.alipio@dlsu.edu.ph, r-jay_relano@dlsu.edu.ph, ryan.vicerra@dlsu.edu.ph, argel.bandala@dlsu.edu.ph, elmer.dadios@dlsu.edu.ph, jonathan.dungca@dlsu.edu.ph

seismic shear wave. The issue here is that it operates from high frequency to ultra-high frequency spectrum that is normally intercepted by other active signals operating on that same band when tested in an urban area. Another disadvantage of GPR is that it is limited to shallow penetration [14-15]. Altering radiation patterns into cylindrical wave emission in a lossy medium resulted in clear near and far field polarizations [16]. Subsurface imaging instruments can therefore increase their applicability in the built environment industry if their operating antenna geometry is optimized.

Quasi-static condition in electrical imaging, by definition, is an irreversible effect that manifests when a very high frequency (VHF) operation attains an induction number of 0 and electrostatic geometric factor of 1 [14]. It is the condition in which the transmitting and receiving antenna is fully capacitively coupled to the ground and can survey the pre-determined skin depth without experiencing signal distortion. Three factors are affecting the quasi-static condition in capacitive coupling to the ground: operating frequency, ground resistivity or conductivity, and geometric conditions [14]. The first and last factors are fixed practical systems, hence, can be altered by the designer. Operating at a very high frequency does not guarantee a quasi-static operation because of the phase rotation of the signal coming to the receiver antenna [14]. Negatively, unoptimized antenna geometry builds up capacitive parasitics that enhance leakage current, increase voltage standing wave ratio (VSWR), and ringing at the terminal of the transmitter [14].

With the need to optimize the antenna configuration, a capacitive dipole has recently been developed. It is normally fabricated in a flat square plate, variably coated with insulating material, and used in a towed-array antenna [14]. To complete the antenna array, this dipole plate is connected to the transmitter or receiver electronic subsystem by dipole wire. Expensive and high resource-consuming antenna design and simulation software that are available in the market, namely Ansoft HFSS, Antenna Magus, CST Microwave Studio, and Altair FEKO, were considered the first practical option to verify if the conceptualized antenna is feasible for application [3, 12, 14, 17]. From a simple axial or inline antenna array, an equatorial antenna has been developed to help improve the resolution of reflected data [14]. This equatorial antenna also enables smooth curve maneuvering when performed in the actual field, but it poses a significantly complicated antenna design compared to the axial configuration. High leakage current and the emergence of the need to perform complex inversion when its dipole spacing is set to greater than 4 m [17]. Another three sets of antenna pairs were needed to be added just to enable imaging when dipole spacing is set to half the dipole length [18]. With these additional challenges in antenna geometry, the S11 pattern of the antenna was used as the basis for determining if the configuration is suitable for such application [19]. Other antenna design techniques involve near-field calibration [20], voltage standing wave ratio minimization [21], trial and error variable placement of electrodes and measurement of resistivity [22] and folding of the antenna along the slot length [23]. Hence, these types of optimization problems are highly aidable to artificial intelligence techniques.

Artificial intelligence (AI) has been useful in the subsurface imaging industry as it births new computational approaches for design optimization [24-26]. Genetic algorithm has been predominantly used for optimizing antenna geometry based on S11 and gain parameters [25], antenna sensitivity and bandwidth [26], and electromagnetic poles properties [24] that are all extracted from other simulation software such as ANSYS Electromagnetics and Altair FEKO. This technique of optimizing the antenna results in a prolonged approach as it requires the designer to perform computation, computer-aided designing, reiterated simulations, and extraction of simulated data. Shown in Table 1 are some of the various existing approaches in antenna design for subsurface imaging.

TABLE I. VARIOUS EXISTING APPROACHES IN ANTENNA DESIGN FOR SUBSURFACE IMAGING

Operating frequency	Dipole type	Antenna configuration	Dipole geometry optimization	Reference
1-25 kHz	Capacitive	Equatorial dipole-dipole	Mathematical	[3]
435 MHz	Capacitive	Axial	Simulator-based	[4]
412-632 MHz	Inductive	Multidisc	VSWR minimization	[21]
0.3-3.8 GHz	Inductive	Single pair	Based on sensitivity and bandwidth	[26]
270-900 MHz	Capacitive	Axial	Based on time-domain obtained GPR waves	[31]

Despite the abovementioned advances in antenna geometry for subsurface imaging and the subsequent techniques to optimize it (Table 1), still there are needs to be improved in the faculty of straight-forward design optimization. It is noticeable that even with using genetic algorithm, the input to that model is not antenna dimensions [25]. Because of this, the conventional approach entails the additional step after optimizing S11 and electromagnetic features instead of directly setting the antenna geometry parameters to be optimized as input to the AI model. Mathematical approach proposed by [14] involves six steps which are the computation of the operating frequency based on the desired skin depth, induction number based on dipole spacing and skin depth, electrostatic geometric factor based on antenna geometry, upper frequency threshold based on antenna geometry and ground resistivity, capacitance modeling of plate and wire antenna sections, and the lower frequency threshold based on antenna electrode dimension [14]. Also, antenna sensitivity has been the normal basis for optimizing antenna and not the more inclusive quasi-static principle including induction number and electrostatic geometric factor. Based on Table 1, a capacitive equatorial dipole-dipole antenna operating at VHF is not yet explored making the current study an addition to the subsurface imaging field. As of this writing, no other AI algorithm has been used aside from the genetic algorithm for this problem making the more advanced evolutionary strategy algorithm recommendable for the current study.

To address these challenges, the main objective of this study is to develop a new technique for optimizing the geometry of a single pair equatorial dipole-dipole antenna for capacitive coupling at 38 MHz to the ground using evolutionary computing. This is necessary to attain the quasi-static condition for subsurface tomography of buried utilities at 1.2 m based on the induction number (value of 0) and electrostatic geometric factor (value of 1). Multigene genetic programming (MGGP) was used to construct the fitness function composed of selected antenna parameters, namely dipole spacing, dipole length, and plate elevation, that have a direct impact on induction number and geometric factor. The suitability of the genetic algorithm and evolutionary strategy were explored in optimizing these antenna geometry parameters as these evolutionary computing metaheuristics pose a clear advantage in optimizing engineering systems [27-29] other than antenna systems for underground imaging making this an initial study and an innovative approach for this field. There are other optimization algorithms like the red fox, polar bear, and chimp optimizers, however, they have fewer hyperparameters which initially resulted in premature convergence making them not an option for this further exploration in this study.

The current study contributes to the following:

1) development of a computational intelligence-based model and technique for faster determination of optimal antenna geometry which avoids the long mathematical computation [14] during antenna geometry modeling;
2) solving the issue of discrete assignment of values during trial-and-error computation by providing the global best solution for dipole spacing, dipole length and dipole elevation from the ground as the equatorial dipole-dipole antenna is intended for subsurface imaging with corresponding induction number and electrostatic geometric factor approaching 0 and 1 respectively;
3) simulation, characterization and elucidation of electric field strength and 38 MHz electromagnetic radiation in the near field radiation with sample metallic object beneath surface and the gain expression in the far-field region; and
4) establishment of dipole spacing and dipole length relationship to attain quasi-static condition. This study presents a novel approach in the aspect of optimizing equatorial dipole-dipole antenna operating at very high frequency for subsurface utility imaging.

2. MATERIALS AND METHODS

Evolutionary computing through genetic algorithm and evolutionary strategy is the core approach employed in this study to optimize the single pair equatorial dipole-dipole antenna geometry (dipole length, dipole spacing, and plate elevation) by achieving the requirement of quasi-static condition in capacitive resistive coupling described by [14]. To generate the optimum combination of selected antenna geometry, five specific steps should be done: determination of antenna dipole type and antenna configuration, the definition of skin depth and operating frequency, extrapolation of antenna geometry parameters, application of symbolic genetic programming to construct the fitness function, and optimization of antenna geometry using two evolutionary computing algorithms (Fig. 1). The output of this approach is the ideal values of dipole length, dipole spacing, and plate elevation and its characterization with induction number and electrostatic geometric factor. The computational intelligence software used in this study was MATLAB.

A. Determination of Antenna Dipole Coupling Type and Antenna Configuration

Capacitive antenna dipole was chosen because of its practicality as other options such as galvanic and inductive are invasive. Galvanic antenna dipole requires hole boring in the ground to penetrate the current and inductive antenna dipole is used for high frequencies and low resistivity which is the opposite of capacitive coupling. On the other hand, capacitive coupling is non-destructive when tested in road imaging and can operate

in the very high frequency spectrum which is not normally used in urban regions. For antenna configuration, equatorial dipole-dipole (Fig. 2a) was selected instead of the axial or inline array because of its high sensitivity in the reception of the reflected signals from underground. Hence, capacitive equatorial dipole-dipole antenna suits the criteria for road tomography. With this antenna configuration, dipole spacing (r, m) is the separation of transmitter and receiver dipole lines (Fig. 2a) and dipole length (l, m) is the span of line dipole connecting the two plate dipoles (Fig. 2a). Plate elevation (h, m) is the thickness of the plate's coating material (Fig. 2b).

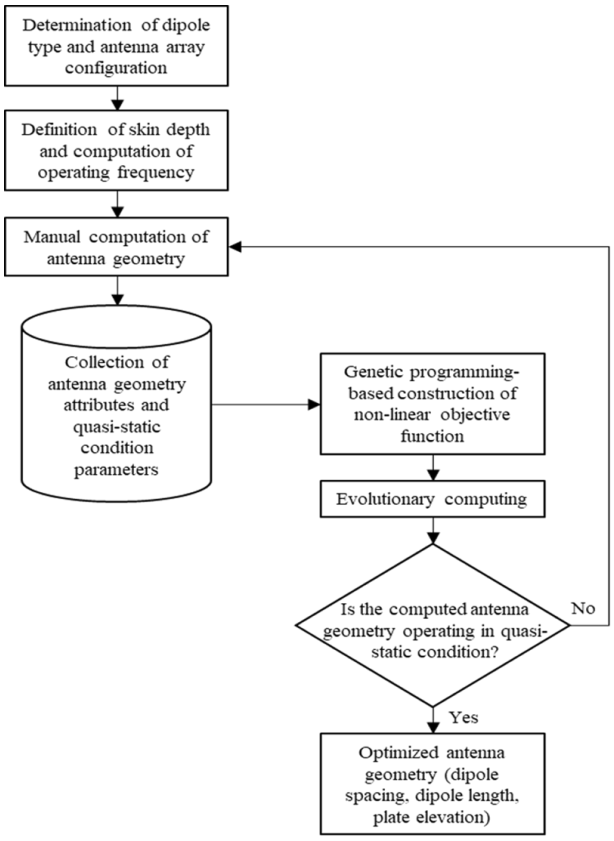

Figure 1. The developmental architecture of the evolutionary computing-based optimization of equatorial dipole-dipole antenna.

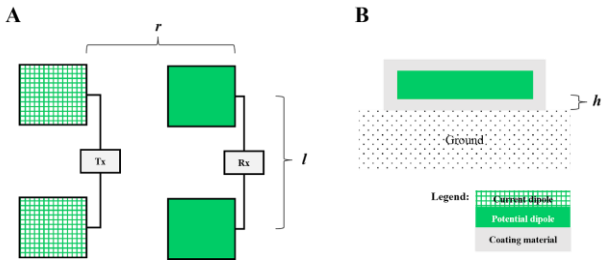

Figure 2. Single-pair equatorial dipole-dipole antenna configuration: (a) top view and (b) front view of a single dipole contact with the ground.

B. Definition of Skin Depth and Computation of Operating Frequency

Skin depth (δ) is the practical depth of investigation in electrical imaging. In subsurface imaging, it is measured from the point of emission (transmitter dipole) to the maximum range the current goes underground. Operating frequency (f, Hz) is directly proportional to ground resistivity (ρ, Ω-m) and is inverse to the square of skin depth in meters and a factor of 500 (1). In this study, the typical ground resistivity of the road was set to 200 Ω-m [14], target skin depth was set to 1.2 m as advised by the Manila Water Company, Inc. (Philippines) to survey buried utilities along with the horizontal infrastructure like water pipes, and the computed operating frequency is 38 MHz. Based on the National Radio Frequency Allocation Table (NRFAT) revision 2019 of the Philippine National Telecommunications Commission, frequencies around 38 MHz are used for short-range devices (SRDs). Hence, a skin depth of 1.2 m and an operating frequency of 38 MHz are suitable for this study.

$$f = \frac{\rho}{(\frac{\delta}{500})^2} \quad (1)$$

C. Extrapolation of Antenna Geometry Parameters

In designing a capacitive resistive equatorial dipole-dipole antenna, a quasi-static condition through induction number (β_{eq}) and electrostatic geometric factor (K_{eq}) should be optimized. The induction number, unitless, is defined by the ratio of dipole spacing (r, m) and skin depth (δ, m) (2). It is described to be useful when the characteristic distances used must be small compared with the electromagnetic skin depth. The electrostatic geometric factor, unitless, is derived by the combinations of dipole spacing, dipole length (l, m), and plate elevation (h, m) (3). Negligible value of geometric factor corresponds to strong signal distortion. Given these standard equations used in designing equatorial antenna, sensitivity analysis in the "What-If Analysis" tool of MS Excel was used in extrapolating the induction number and geometric factor by providing combinations of

predictors (antenna geometry parameters). In this study, the following permissible ranges were set to establish the considerable practical fitness functions: 0.5 m ≤ r < 2 m, 0.5 m ≤ l < 2 m, and 0.001 m ≤ h < 0.01 m. Overall, there are 160 combinations of predictors.

$$\beta_{eq} = \frac{r}{\delta} \tag{2}$$

$$K_{eq} = \frac{\frac{1}{\sqrt{r^2+4h^2}} - \frac{1}{\sqrt{r^2+l^2+4h^2}}}{\frac{1}{r} - \frac{1}{\sqrt{r^2+l^2}}} \tag{3}$$

D. *Construction of Objective Functions Using Genetic Programming*

Both the induction number and the geometric factor are determinants of capacitive coupling of the transmitter and receiver antennas to the ground. Multigene symbolic regression genetic programming (MSRGP) is an evolutionary algorithm (EA) that evolves on a genetic search approach for both the mathematical topology and genetic parameters by following the pseudocode 1 (Fig. 3) [27]. This approach enables lower depth smaller trees containing the individual genes of the expression to evolve. Unlike other regression and predictive computational intelligence models, MSRGP outputs a symbolic and explanatory model. In this study, MSRGP was applied using the GPTIPS version 2 application of MATLAB R2020a. The extrapolated antenna geometry parameters were used as input to the multi-objective MSRGP. The MSRGP model was configured using 100 population size, 100 generations, tournament selection size of 50, elite fraction of 0.1 with lexicographic selection pressure, crossover rate of 0.85, mutation rate of 0.16, 10 maximum number of genes, maximum tree depth of 5, and the mathematical function nodes limited to ['times', 'minus', 'plus', 'sqrt', 'square', 'sin', 'cos', 'add3', 'mult3', 'log', 'cube', 'neg', 'abs']. MSRGP terminates when the computed individual fitness function is below 1e-3. The antenna electrical parameters that are to be optimized are the induction number and electrostatic geometric factor to attain quasi-static condition for functional subsurface imaging. Complying with the quasi-static condition manifests correct transmitter antenna radiation and receiver handshake.

The developed MSRGP model for induction number has 4 genes with R^2 of 1 (4) and R^2 of 0.99909 for the geometric factor (5). For both generated models, x_1 is the dipole spacing (r), x_2 is the dipole length (l), and x_3 is plate elevation (h). These models characterize the antenna electrical system as changing any of the r, l, or h geometric antenna parameters has a corresponding impact on the electromagnetic performance manifested by electric field radiation pattern and power loss. Hence, β and K expressions in (4) and (5) are used as objective functions for optimizing the corresponding induction number and electrostatic geometric factor.

Pseudocode 1: Genetic Programming

```
1:  Initialize the first generation
2:  Conversion of binary tree to expression
3:  Individual fitness evaluation
4:  if end criterion is not met do
5:      Selection
6:      Crossover and mutation
7:      Generation of new individual (gen = gen + 1)
8:      Go to step 2
9:  else return symbolic expression with best fitness
10: end
```

Figure 3. Pseudocode of multigene symbolic regression genetic programming for constructing the fitness functions of induction number and electrostatic geometric factor.

$$\beta = 0.01\, x_1 + 1.02e^{-18}\, x_2 - 1.015e^{-17}\, x_3 + 1.05e^{-17} \tag{4}$$

$$K = 5.25e^{-5}\, x_1 + 2.3e^{-5}\, x_3 - 5.25e^{-5}\, \sin(x_1 + x_2 + x_3) - 9.08e^{-5}\, \mathrm{abs}(x_3) + 9.08e^{-5}\, \cos(x_1) + 2.3e^{-5}\, \log(x_1) - 3.49e^{-5}\, \mathrm{abs}(x_3 + \log(x_1) + x_2^2) - 22.5\, x_3^2\, \cos(x_1) - 37.8\, x_3^2\, \cos(x_1)^4 + 19.4\, x_3^3\, \cos(x_1)^3 + 2.3e^{-5}\, x_2^2 - 0.508\, x_3^2 - 5.28 x_2^2\, x_3^2\, \cos(x_1)^3 + 57.2\, x_1\, x_3^2\, \cos(x_1)^3 + 19.4\, x_2\, x_3^2\, \cos(x_1)^3 + 0.532\, x_1\, x_2^2\, x_3^2\, \cos(x_1)^2 + 4.74\, x_1\, x_2^2\, x_3^2\, \mathrm{abs}(x_3)\cos(x_1) + 1.0 \tag{5}$$

E. *Optimization of Antenna Geometry Using Evolutionary Computing*

To attain the quasi-static condition in the capacitive coupling, the induction number must be approaching 0 and the electrostatic geometric factor must be approaching 1. The mathematical topology of the fitness functions of induction number and geometric factor is defined by $\beta = f\{\mathrm{b}\,(r, l, h)\}$ and $K = f\{\mathrm{k}\,(r, l, h)\}$ where b and k represent the mathematical complexity that is previously defined in (4) and (5), respectively. These fitness functions define the desirability of an optimization solution. In this study, evolutionary computing through a genetic algorithm (GA) and evolutionary strategy (ES) was employed to optimize the induction number by utilizing minimization and maximization for the electrostatic geometric factor. The result of these optimizations is the ideal combination of antenna parameters.

Genetic algorithm starts with employing real value encoding of the three chromosomes (r, l, h) which is a combination of genes that allows this algorithm to

generate the best solution (Fig. 4, Pseudocode 2). These chromosomes form the initial population which was fixed at 50. To ensure the exploration and exploitation of GA over the searchable space, it is equipped with three genetic operators namely selection, crossover, and mutation rates [28]. In this study, a tournament selection was employed in selecting 10 chromosomes and the two chromosomes with the highest fitness value are selected as parents for crossover. The single-point crossover was employed, and it happens when the genes are recombined between parents to create new offspring with unique genetic traits. Mutation occurs when some of the genes of the new offspring are altered based on the mean and standard deviation of gene values of the current generation (g). Both crossover and mutation rates were explored in the range of 0.1 to 1. Elite count and migrate rate were set to 2.5 (5% of initial population) and 1, respectively. The GA cyclically performs fitness value evaluation, selection, crossover, and mutations as long as the current generation is below the maximum generation of 100 or if the chromosome best fitness is less than the maximum fitness of $1e^{-6}$ (Fig. 4).

Covariance matrix adaptation evolutionary strategy (CMA-ES) is an advanced type of ES employed in this study to avoid early local convergence [29]. Its selection and adaption process is based on the parameterized multivariate normal distribution (PMND) that considers the convergence of the previous generation through a covariance matrix (C). The evolutionary process of CMA-ES starts with generating the chromosomes, updating the best solution, sorting the population, crossover, and updating the mean and the covariance based on (6), Gaussian mutation, and selection (Fig. 4, Pseudocode 3). The Gaussian mutation is based on the individual chromosomes (x) in optimizing the offspring of the next generation (g+1) that is affected by weights (w), initial chromosome count (k) where λ is denoted as maximum count, the standard deviation of fitness value (σ), and covariance matrix (6). Here, the explorative ranges of genetic operators of CMA-ES are set identical to GA.

Because real-valued chromosome encoding was employed, GA and CMA-ES output the best solution for optimizing the two fitness functions (4) and (5) in terms of the actual real-valued number in meters. To determine the recommended antenna parameter based on the outputs of genetic algorithm and evolutionary strategy, the induction number and geometric factor were recalculated using the standard formulas (2) and (3). The combination that is closest to the quasi-static condition requirement was selected as ideal. Note that the best fitness value during convergence in GA and CMA-ES can be partially visualized in the interaction of varying genetic crossover and mutation rates (Fig. 5). The best antenna geometry generated by these evolutionary algorithms was designed using SolidWorks and simulated using Altair FEKO software.

Pseudocode 2: Genetic Algorithm

1: Set the chromosomes of single pair antenna geometry (dipole length, dipole spacing, and plate elevation)
2: Set GA hyperparameters (crossover, mutation, selection, elite count, and migration rates)
3: Generate the initial population
4: **while** generation < MaxGeneration or BestFitness < MaxFitness **do**
5: Fitness value calculation (Eq. 4, 5)
6: **Selection**
7: **Crossover** [A (l_a, r_a+b, h_a+c), B (l_b+a, r_b, h_b+c), C (l_c+a, r_c+b, h_c)]
8: **Mutation** [Ab (l_a, r_a, h_a), Bc (l_b, r_b, h_b), Ca (l_c, r_c, h_c)]
9: **end**

Pseudocode 3: Evolutionary Strategy

1: Set the chromosomes of single pair antenna geometry (dipole length, dipole spacing, and plate elevation)
2: Set ES hyperparameters (crossover, mutation, and selection rates)
3: Generate the initial population
4: **while** generation < MaxGeneration or BestFitness < MaxFitness **do**
5: **Crossover** [A (l_a, r_a+b, h_a+c), B (l_b+a, r_b, h_b+c), C (l_c+a, r_c+b, h_c)]
6: **Gaussian mutation** [Ab (l_a, r_a, h_a), Bc (l_b, r_b, h_b), Ca (l_c, r_c, h_c)]
7: Fitness value calculation (Eq. 4, 5)
8: **Selection**
9: **end**

Figure 4. Pseudocodes for genetic algorithm and evolutionary strategy processes in optimizing the induction number and electrostatic geometric factor fitness function of a single pair equatorial dipole-dipole antenna.

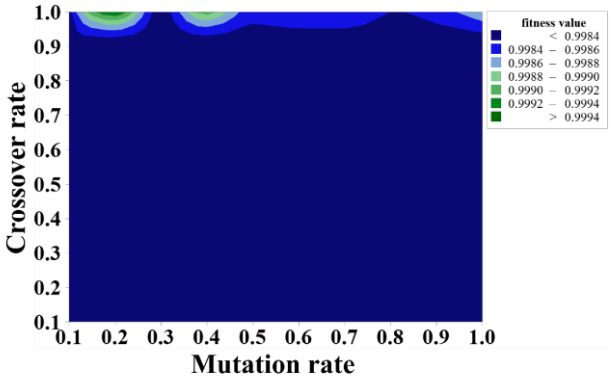

Figure 5. Sample contour map of the impact of varying crossover and mutation rates as partial determinants of fitness value in optimizing electrostatic geometric factor using genetic algorithm.

3. RESULTS AND DISCUSSION

A. Induction Number and Electrostatic Geometric Factor Characterization

The more conventional approach to designing an antenna for electrical imaging is through long and time-consuming mathematical calculations [14] and extraction of antenna electromagnetic parameters from commercial software in tandem with the genetic algorithm [24, 15] which are completely different from the straightforward quasi-static condition determinant as a function of antenna geometry allied with evolutionary computing approach developed in this study (Fig. 1). Using Pearson's correlation analysis (PCC) with 95% confidence, increasing the antenna dipole spacing has a positive impact on the induction number while dipole length has no significant impact on the unoptimized geometry (Table 2). Interestingly, there was a significant difference between the unoptimized and optimized antenna as the

latter has a weak linear relationship to induction number and geometric factor.

TABLE II. PEARSON CORRELATIONS OF ANTENNA GEOMETRY PARAMETERS INFLUENCING THE QUASI-STATIC CONDITION IN SUBSURFACE IMAGING USING AN EQUATORIAL DIPOLE-DIPOLE ANTENNA IN VERY HIGH FREQUENCY SPECTRUM (B IS INDUCTION NUMBER, K IS THE GEOMETRIC FACTOR, R IS DIPOLE SPACING, L IS DIPOLE LENGTH, H IS PLATE ELEVATION)

Antenna Geometry Condition	$\frac{\beta}{r}$	$\frac{\beta}{l}$	$\frac{K}{r}$	$\frac{K}{h}$	$\frac{l}{r}$
Unoptimized	1	0	0.123	-0.547	0
Optimized	0.011	-0.159	0.079	0.019	0.133

On average, dipole spacing, and length should be increased by a factor of 1.250 for every unit of geometric factor and 100 for every unit increase in induction number based on the developed quasi-static dynamic maps (Figs. 6a and 6b). Plate elevation should be increased by a factor of $5.501e^{-3}$ for every unit of geometric factor and 0.440 for every unit increase in induction number (Fig. 6c). Taken together, these results suggest that for a scaled-down antenna geometry, the induction number is approaching 0.005 and the geometric factor is approaching 0.9985. These determined quasi-static condition determinants agree with the established standard [14].

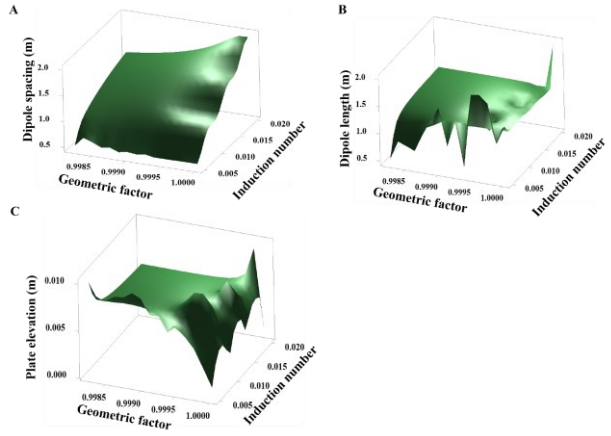

Figure 6. Quasi-static dynamic maps of induction number and electrostatic geometric factor in relation to major equatorial antenna geometry parameters: (a) dipole spacing, (b) dipole length, and (c) plate elevation using Minitab R18 software.

B. *Optimized Geometry of Equatorial Dipole-Dipole Antenna*

After several exploitations and exploration over the search space of antenna geometry, *β-GA* and *K-GA* showed fast exploration and prolonged exploitation as shown in the corresponding fitness curve (Figs. 7a and 7b) while *β-ES* and *K-ES* showed slow exploration and fast exploitation of the global best solution (Figs. 7c and 7d). From the perspective of computational intelligence, it can be noticed that optimization performances of both GA and CMA-ES are almost identical as depicted by the constructed surface curves of the three antenna geometries (Fig. 7).

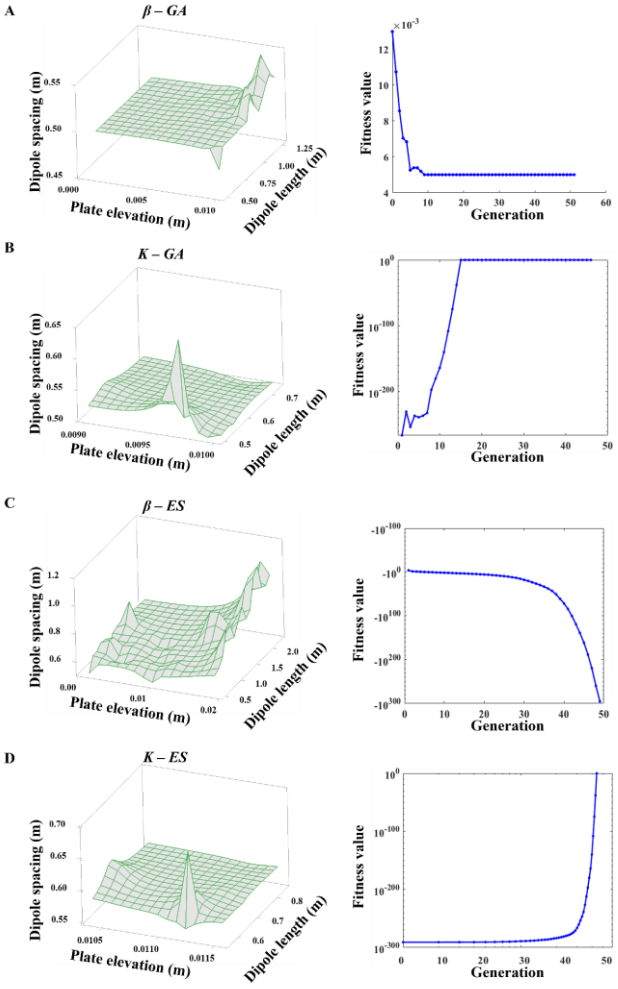

Figure 7. Optimized antenna geometry parameter relationships and corresponding fitness curve generated by genetic algorithm (GA) and evolutionary strategy (ES). β is the induction number and K is the electrostatic geometric factor. (a) *β-GA*, (b) *K-GA*, (c) *β-ES*, and (d) *K-ES*.

By using the genetic algorithm to meet a β approaching 0 and a K approaching 1, the resulting antenna geometry for dipole spacing and length are identical with a measurement of 0.5 m (Table 3). Hence, resolving that *β-GA* and *K-GA* have met the global optimum. On the other hand, by using the evolutionary strategy, it is noticeable that dipole length and spacing are identical for β which is 0.5075 m, and for K it is 0.5067 m (Table 3). A possible explanation for these results is that the genetic programming-generated fitness function for β

(4) and *K* (5) is different. The default, GA-optimized, and ES-optimized antennas were modeled (Fig. 8) in Altair Feko software following the obtained geometries in Table 3 with a 10 W 1 kV transmitter source and a steel pipe placed and aligned at 1.2 m beneath the surface of dipole electrodes representing an industrial utility under the road. Through electrical analysis at 38 MHz emission, the default antenna exhibited power loss that is 106.304% and 131.048% higher than the GA and ES-based antennas respectively. On the other hand, the ES-optimized antenna resulted in the highest efficiency of 97.38% followed by the GA-optimized antenna which is 96.76%. On the question of what optimal antenna geometry should be used, this study found out that antenna dipole space and length should be numerically equal (7), and the plate elevation should be ≤ 0.0112 m or technically 2.24% of *r* (Table 2) to attain the quasi-static condition.

Near-field and far-field radiations for the default, GA- and ES-optimized antennas confirmed that using computational intelligence approach in optimizing antenna geometry eliminates the possibility of misaligning the peak radiation power onto the surface of the utility as depicted in the default antenna (Fig. 8a). The reflected radiation to the receiver of the default antenna characterizes deviation or missing the spot of the buried utility (Fig. 9). The electric field crests outside the metallic pipe making the default antenna geometry unreliable for mapping buried utilities in 38 MHz operations. Whereas, the antennas constructed based on the recommendations of GA and ES appeared to be sensitive enough to the buried metallic pipe by concentrating its radiation with a high electric field on the target's surface (Fig. 8b and 8c, Fig. 9). It can be noticed that these high electric field areas are expressed in the near field regions that are directly perpendicular to the transmitter dipoles with a maximum value of 75 to 80 dBV m^{-1} for GA and ES antennas while the default antenna has 4.0 dBV m^{-1}. Aside from the significance of antenna geometry, an important implication of this finding is that timing is very important when performing moving road tomography. Far-field radiation is shown in Fig. 8 with the highest total gain of 3 dBi for both default and GA-optimized antennas while ES-optimized antennas have a gain of 4 dBi. This total gain can be considered acceptable given that the dipole plates were not coated with any dielectric which can be considered one of the limitations of this current study. The reason why plate elevation should be closer to the ground is to avoid the added capacitive parasitic that may exist because of the air gap. To avoid the negative impact of parasitics on the total capacitance of the antenna system, increase in VSWR, and ringing at the end of the transmitter, dipoles are buried underground for galvanic coupling [3, 12, 14, 17], however, that approach is not the best to implement as it is destructive. By using capacitive resistive imaging for underground imaging as proposed in this study, current and potential dipole plates can be coated with epoxy, acrylic, or other non-conductive materials [30]. The thickness of the coating material resembles the plate elevation; thus, it is the separator from the dipole metal plate to the ground or road. Overall, this approach of using computational intelligence (Fig. 1) proves to be a good complement to the long method of computations and the use of expensive simulators to determine the optimum antenna geometry that can operate in quasi-static conditions for capacitive coupling to the ground.

$$\textit{Dipole spacing} \approx \textit{dipole length} \tag{7}$$

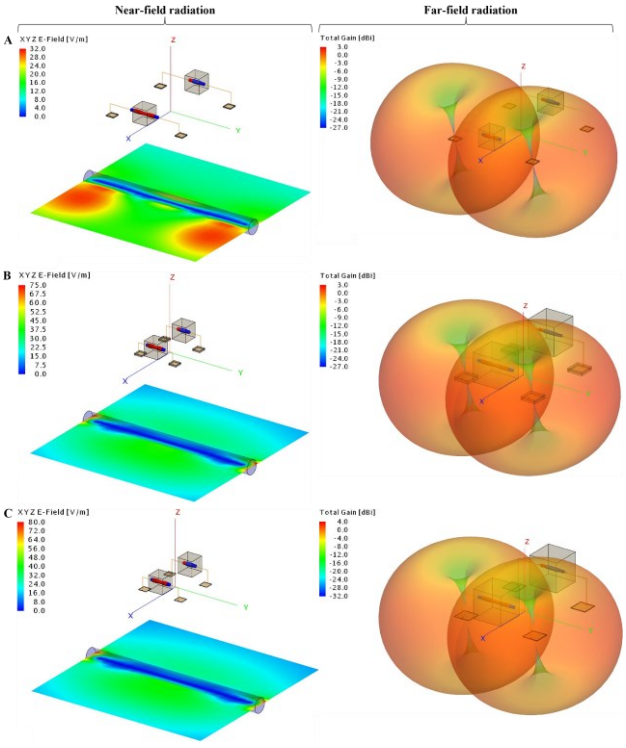

Figure 8. Altair FEKO-generated total gain expression in the far-field region (left column) and electric field strength expression in the near field radiation with sample metallic object (steel pipe) located 1.2 meters below the antenna dipoles (right column) for (a) default, (b) GA-optimized, and (c) ES-optimized antenna geometry.

TABLE III. OPTIMIZED SINGLE PAIR EQUATORIAL DIPOLE-DIPOLE ANTENNA GEOMETRY USING CONVENTIONAL APPROACH AND EVOLUTIONARY COMPUTING MODELS WITH POWER LOSS AND EFFICIENCY RATINGS

Evolutionary Computing Model	For Induction Number			For Geometric Factor			Power Loss (mW)	Efficiency
	Dipole spacing (m)	*Dipole length (m)*	*Plate elevation (m)*	*Dipole spacing (m)*	*Dipole length (m)*	*Plate elevation (m)*		
Default	1.0000	1.0000	0.0056	1.0000	1.0000	0.0056	344.0	0.9656
Genetic algorithm	0.5000	0.5000	0.0100	0.5000	0.5000	0.0100	323.6	0.9676
Evolutionary strategy	0.5075	0.5075	0.0010	0.5067	0.5067	0.0112	262.5	0.9738

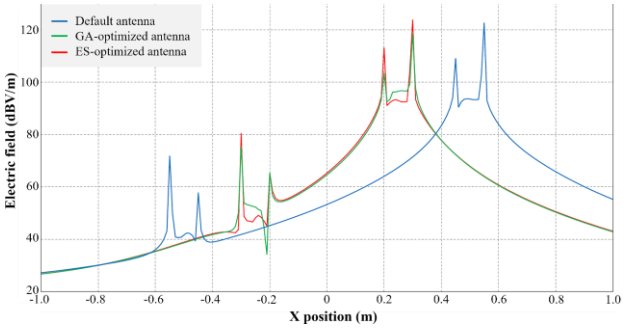

Figure 9. Trends of near field electric field radiation with sample metallic object (steel pipe) located 1.2 meters below the antenna dipoles (right column) for default, GA-optimized, and ES-optimized antenna geometry.

The current study has found out that capacitive resistivity antenna geometry can be optimized using computational intelligence which resulted in more accessible parameters unlike simulating the design and doing trial and error in readjustments of the design that is the dominant approach of the previous studies done by [18-19, 22-23]. The most significant applied geophysics-relevant finding was the establishment of the relation between dipole spacing and dipole length (7) to attain the high probability for ground capacitive coupling which could only happen when quasi-static conditions of induction number and electrostatic geometric constant were met. An implication of this is the possibility that an antenna for road tomography can be lowered in elevation to avoid more capacitive and inductive parasitics due to air gap but it requires more adjustments in the design of the mechanical trailer as the antenna now is close to the ground that may be hit by debris on the ground. Likewise, lowering the antenna elevation implies a change in antenna capacitance. This study proposes that this established relationship of dipole-dipole antenna geometry is only applicable for an equatorial antenna configuration. By adjusting the antenna geometry based on the resulting voltage standing wave ratio as proposed by [21], the directivity gain and reflection at the plate were also modified. Given the fact that voltage standing wave ratio is significantly affected by the signal reflection that is materialized through a mismatch transmitter and antenna, antenna geometry should be optimized more particularly in an equatorial dipole-dipole setup as the total capacitance of the antenna system is substantially dynamic when the elevation of wire antenna section was changed. The results of this study significantly differ from the outputs provided by [4, 21, 26, 31] as they have explored on capacitive type of dipole but all of them have operated above and below the very high frequency spectrum which is our target frequency of operation. Near field and far field operation as proposed by [20, 32] was also performed here through Altair FEKO simulation of default and optimized antennas. Some of the issues emerging from these findings relate specifically to capacitance modeling of an equatorial dipole-dipole antenna which can also be modeled and optimized using evolutionary computing [33]. However, more research on subsurface imaging and antenna geometry optimization for road tomography needs to be undertaken like the association of operating frequency, the capacitance of the total antenna system, and the natural resistivity of ground in different climates and geographical locations. Hence, it was proven that evolutionary computing through genetic algorithm and evolutionary strategy was effective as an optimization technique for this application.

4. CONCLUSION

This study has presented a newly developed technique for optimizing the geometry of a single pair equatorial

E-mail: ronnie.concepcion@dlsu.edu.ph, jonah_baun@dlsu.edu.ph, adrian_janairo@dlsu.edu.ph, melchizedek.alipio@dlsu.edu.ph, r-jay_relano@dlsu.edu.ph, ryan.vicerra@dlsu.edu.ph, argel.bandala@dlsu.edu.ph, elmer.dadios@dlsu.edu.ph, jonathan.dungca@dlsu.edu.ph

dipole-dipole antenna for capacitive coupling to the ground using evolutionary computing. To attain the quasi-static condition, the fitness functions for induction number and electrostatic geometric factor as a function of antenna geometry were constructed using multigene genetic programming and explored and exploited using genetic algorithm and evolutionary strategy to generate the best combination of antenna parameters. Based on the results, two considerations were established in designing such antenna configuration: the dipole spacing and length should be equal in measurement, and the plate elevation should be 2.24% of the dipole spacing value. This very low plate elevation minimizes the high dielectric due to air resulting in a reduction in parasitic and void ringing at the end of the transmitter. The issue of discrete assignment of antenna geometry values was also solved as manifested in the results of GA and ES optimizations. It was also confirmed that there is a comparatively low power loss and high efficiency for GA- and ES-optimized antennas than the default antenna at 38 MHz operations. Overall, despite the novel aspect and exploratory nature of using computational intelligence in optimizing antenna geometry operating at very high frequency for subsurface utility imaging, the process of attaining such goal is shortened and became more precise. There will be no need to use another simulator to readjust the antenna design and no long mathematical solution is necessary. For future studies, capacitance modeling of the antenna should be explored based on the same antenna geometry parameters and other bio-inspired algorithms like jellyfish swarm, bald eagle search, and African vultures optimizations.

ACKNOWLEDGMENT

This study is supported by the Engineering Research and Development for Technology and the Philippine Council for Industry, Energy, and Emerging Technology Research and Development (PCIEERD) of the Department of Science and Technology, and the Office of the Vice President for Research and Innovation of De La Salle University, Manila. Also, appreciation to Milo Rivera for the technical support.

REFERENCES

[1] D. Carbonel, V. Rodríguez-Tribaldos, F. Gutiérrez, J. P. Galve, J. Guerrero, M. Zarroca, C. Roqué, R. Linares, J. P. McCalpin, and E. Acosta, "Investigating a damaging buried sinkhole cluster in an urban area (Zaragoza City, NE Spain) integrating multiple techniques: Geomorphological surveys, DInSAR, DEMS, GPR, ERT, and Trenching," Geomorphology, vol. 229, pp. 3–16, May 2015. doi: 10.1016/j.geomorph.2014.02.007.

[2] A. Ruffell and R. Parker, "Water penetrating radar," Journal of Hydrology, vol. 597, p. 126300, Oct. 2021. doi: 10.1016/j.jhydrol.2021.126300.

[3] E. Tsiogas, I. Kostavelis, G. Kouros, A. Kargakos, D. Giakoumis, and D. Tzovaras, "Surface exploration with a robot-trailer system for autonomous subsurface scanning," in 2019 IEEE SmartWorld, Ubiquitous Intelligence & Computing, Advanced & Trusted Computing, Scalable Computing & Communications, Cloud & Big Data Computing, Internet of People and Smart City Innovation (SmartWorld/SCALCOM/UIC/ATC/CBDCom/IOP/SCI), Aug. 2019, pp. 1498–1503. doi: 10.1109/SmartWorld-UIC-ATC-SCALCOM-IOP-SCI.2019.00080.

[4] Y. Wang, G. Cui, and J. Xu, "Semi-automatic detection of buried rebar in GPR data using a genetic algorithm," Automation in Construction, vol. 114, p. 103186, Nov. 2020. doi: 10.1016/j.autcon.2020.103186.

[5] M. O. Cimpoiaşu, O. Kuras, T. Pridmore, and S. J. Mooney, "Potential of geoelectrical methods to monitor root zone processes and structure: A Review," Geoderma, vol. 365, p. 114232, Nov. 2020. doi: 10.1016/j.geoderma.2020.114232.

[6] M. S. Dizaji, M. Alipour, and D. K. Harris, "Subsurface damage detection and structural health monitoring using digital image correlation and topology optimization," Engineering Structures, vol. 230, p. 111712, Feb. 2021. doi: 10.1016/j.engstruct.2020.111712.

[7] F. Garcia-Garcia, A. Valls-Ayuso, J. Benlloch-Marco, and M. Valcuende-Paya, "An optimization of the work disruption by 3D cavity mapping using GPR: A new sewerage project in Torrente (Valencia, Spain)," Construction and Building Materials, vol. 154, pp. 1226–1233, Sep. 2017. doi: 10.1016/j.conbuildmat.2017.06.116.

[8] P. Sentenac, V. Benes, V. Budinsky, H. Keenan, and R. Baron, "Post flooding damage assessment of Earth dams and historical reservoirs using non-invasive geophysical techniques," Journal of Applied Geophysics, vol. 146, pp. 138–148, Dec. 2017. doi: 10.1016/j.jappgeo.2017.09.006.

[9] H. Song, D.K. Woo, and Q. Yan, "Detecting subsurface drainage pipes using a fully convolutional network with optical images," Agricultural Water Management, vol. 249, p. 106791, Oct. 2021. doi: 10.1016/j.agwat.2021.106791.

[10] K. Agred, G. Klysz, and J.-P. Balayssac, "Location of reinforcement and moisture assessment in reinforced concrete with a double receiver GPR antenna," Construction and Building Materials, vol. 188, pp. 1119–1127, Aug. 2018. doi: 10.1016/j.conbuildmat.2018.08.190.

[11] G. Kouros, I. Kotavelis, E. Skartados, D. Giakoumis, D. Tzovaras, A. Simi, and G. Manacorda, "3D underground mapping with a mobile robot and a GPR antenna," in 2018 IEEE/RSJ International Conference on Intelligent Robots and Systems (IROS), Oct. 2018, pp. 4717–4722. doi: 10.1109/IROS.2018.8593848.

[12] M. Mifkovic, A. Swidinsky, and M. Mooney, "Imaging ahead of a tunnel boring machine with DC resistivity: A laboratory and numerical study," Tunnelling and Underground Space Technology, vol. 108, p. 103703, Feb. 2021. doi: 10.1016/j.tust.2020.103703.

[13] T. Hayashi, N. Mori, and T. Ueno, "Non-contact imaging of subsurface defects using a scanning laser source," Ultrasonics, vol. 119, p. 106560, Jan. 2022. doi: 10.1016/j.ultras.2021.106560.

[14] O. Kuras, "The capacitive resistivity technique for electrical imaging of the shallow subsurface," Ph.D. dissertation, University of Nottingham, Nottingham, UK, 2002.

[15] S. Mackens, N. Klitzsch, C. Grützner, and R. Klinger, "Quaternary sediment architecture in the Orkhon Valley (Central Mongolia) inferred from capacitive coupled resistivity and Georadar measurements," Geomorphology, vol. 292, pp. 72–84, Sep. 2017. doi: 10.1016/j.geomorph.2017.05.002.

[16] F. Frezza, L. Pajewski, C. Ponti, G. Schettini, and N. Tedeschi, "Cylindrical-wave approach for electromagnetic scattering by subsurface metallic targets in a lossy medium," Journal of Applied Geophysics, vol. 97, pp. 55–59, Apr. 2013. doi: 10.1016/j.jappgeo.2013.01.004.

[17] Ç. Balkaya, Ü. Y. Kalyoncuoğlu, M. Özhanlı, G. Merter, O. Çakmak, and İ. Talih Güven, "Ground-penetrating radar and electrical resistivity tomography studies in the biblical Pisidian

Antioch City, Southwest Anatolia," Archaeological Prospection, vol. 25, pp. 285–300, Jul. 2018. doi: 10.1002/arp.1708.

[18] O. Souza de Araújo, E. Chemas Hindi, A. Rigoti, and F.H. Rigoti, "Improved Imaging of a karst aquifer using focused source electromagnetic and differentially normalized method: A qualitative analysis," Geophysical Prospecting, vol. 67, pp. 1965–1976, Nov. 2019. doi: 10.1111/1365-2478.12795.

[19] L. Wang, "Analysis and development of components of dipole linear antenna array," in 2017 IEEE 17th International Conference on Communication Technology (ICCT), Oct. 2017, pp. 1005–1008. doi: 10.1109/ICCT.2017.8359730.

[20] L. Bannawat, A. Boonpoonga, and S. Burintramart, "Resolution improvement of GPR image using antenna calibration for object detection," in 2017 International Symposium on Antennas and Propagation (ISAP), Oct. 2017, pp. 1–2. doi: 10.1109/ISANP.2017.8228990.

[21] A. V. Kochetov, G. V. Komarov, and D. Y. Kulikova, "Ultra-wideband multidisc antenna with reconfigurable polarization for ground-penetrating imaging radar," in 2019 IEEE Conference of Russian Young Researchers in Electrical and Electronic Engineering (EIConRus), Feb. 2019, pp. 375–380. doi: 10.1109/EIConRus.2019.8657062/LAWP.2011.2121051.

[22] P.B. Wilkinson, S. Uhlemann, J.E. Chambers, P.I. Meldrum, and M.H. Loke, "Development and testing of displacement inversion to track electrode movements on 3-D electrical resistivity tomography monitoring grids," Geophysical Journal International, vol. 200, pp. 1566–1581, Sept. 2015. doi: 10.1093/GJI/GGU483.

[23] W. Kang, S. Lee, and K. Kim, "A ground-folded slot antenna for Imaging Radar Applications," IEEE Antennas and Wireless Propagation Letters, vol. 10, pp. 155–158, Feb. 2011. doi: 10.1109.

[24] A. De Coster and S. Lambot, "Full-wave removal of internal antenna effects and antenna–medium interactions for improved ground-penetrating radar imaging," IEEE Transactions on Geoscience and Remote Sensing, vol. 57, pp. 93–103, Jan. 2019. doi: 10.1109/TGRS.2018.2852486.

[25] A. Srivastav, P. Nguyen, M. McConnell, K.A. Loparo, and S. Mandal, "A highly digital multiantenna ground-penetrating radar (GPR) system," IEEE Transactions on Instrumentation and Measurement, vol. 69, pp. 7422–7436, Dec. 2020. doi: 10.1109/TIM.2020.2984415.

[26] X. Zhuge, T.G. Savelyev, A.G. Yarovoy, and L.P. Ligthart, "Subsurface imaging with UWB Linear Array: Evaluation of antenna step and array aperture," in 2007 IEEE International Conference on Ultra-Wideband, Sept. 2007, pp. 224–229. doi: 10.1109/ICUWB.2007.4380917.

[27] R. Concepcion II, J. Alejandrino, C. H. Mendigoria, E. Dadios, A. Bandala, E. Sybingco, and R. R. Vicerra, "Lactuca sativa leaf extract concentration optimization using evolutionary strategy as photosensitizer for Tio2-filmed Grätzel Cell," Optik, vol. 242, p. 166931, Sep. 2021. doi: 10.1016/j.ijleo.2021.166931.

[28] R. Concepcion II, S. Lauguico, J. Alejandrino, J. De Guia, E. Dadios, and A. Bandala, "Aquaphotomics determination of total organic carbon and hydrogen biomarkers on aquaponic pond water and concentration prediction using genetic programming," in 2020 IEEE 8th R10 Humanitarian Technology Conference (R10-HTC), Dec. 2020, pp. 1–6. doi: 10.1109/R10-HTC49770.2020.9357030.

[29] R. Concepcion II, S. Lauguico, R. R. Tobias, E. Dadios, A. Bandala, and E. Sybingco, "Genetic algorithm-based visible band Tetrahedron Greenness index modeling for Lettuce Biophysical Signature Estimation," in 2020 IEEE REGION 10 CONFERENCE (TENCON), Oct. 2020, pp. 1193–1198. doi: 10.1109/TENCON50793.2020.9293916.

[30] K. Francisco, R. Concepcion II, R.-J. Relano, M. L. Enriquez, J. J. Baun, A. P. Mayol, J. Espanola, R. R. Vicerra, A. Bandala, E. Dadios, A. Ubando, and H. Co, "Analytical hierarchical process-based material selection for trailer body frame of an underground imaging system," in 2021 IEEE 13th International Conference on Humanoid, Nanotechnology, Information Technology, Communication and Control, Environment, and Management (HNICEM), Mar. 2021, pp. 1–5. doi: 10.1109/hnicem54116.2021.9732048.

[31] H. Bai and J. V. Sinfield, "Effects of GPR antenna configuration on subpavement drain detection based on the frequency-shift phenomenon," Journal of Applied Geophysics, vol. 146, pp. 198–207, Dec. 2017. doi: 10.1016/J.JAPPGEO.2017.09.019.

[32] A. G. Janairo, J. J. Baun, R. Concepcion II, R.-J. Relano, K. Francisco, M. L. Enriquez, A. Bandala, R. R. Vicerra, M. Alipio, and E. P. Dadios, "Optimization of subsurface imaging antenna capacitance through geometry modeling using Archimedes, Lichtenberg and Henry Gas solubility metaheuristics," in 2022 IEEE International IOT, Electronics and Mechatronics Conference (IEMTRONICS), Mar. 2022, pp. 1–6. doi: 10.1109/iemtronics55184.2022.9795789.

[33] F. Benedetto and F. Tosti, "GPR spectral analysis for clay content evaluation by the frequency shift method," Journal of Applied Geophysics, vol. 97, pp. 89–96, May 2013. doi: 10.1016/j.jappgeo.2013.03.012.

Ronnie Concepcion II completed his doctoral degree in Electronics & Communications Engineering at De La Salle University Manila, Philippines in 2021. He is an Associate Professor at De La Salle University since 2021. His main research works include the development of non-destructive techniques for crop phenotyping in the molecular, organelle, and system levels using integrated machine vision and computational intelligence for sustainable and precision agriculture.

Jonah Jahara Baun received her bachelor's degree in Electronics Engineering at Polytechnic University of the Philippines Manila, Philippines in 2020 and started pursuing her master's degree in Electronics and Communications Engineering at De La Salle University Manila, Philippines in 2022. Her main research work focuses on the development of a Capacitive Resistivity Underground Imaging System.

Adrian Genevie Janairo received his bachelor's degree in Electronics Engineering at the University of Santo Tomas Manila, Philippines in 2020 and started pursuing his master's degree in Electronics and Communications Engineering at De La Salle University Manila, Philippines in 2022. His main research work focuses on the development of a Capacitive Resistivity Underground Imaging System.

Melchizedek Alipio completed his doctoral degree in Electronics & Communications Engineering at the University of the Philippines Diliman in 2018. He is an Associate Professor at De La Salle University. His research interests include Wireless Sensor Networks, Machine Learning and Information Processing, Smart Cities, and Agriculture.

R-jay Relano received his bachelor's degree in Mechanical Engineering at Bulacan State University Bulacan, Philippines in 2010 and started pursuing his Master's degree in Manufacturing Engineering and Management at De La Salle University Manila Philippines in 2021. His main research work focuses on designing the mechanical component of a towed imaging system.

Ryan Rhay Vicerra completed his doctoral degree in Electronics & Communications Engineering at De La Salle University Manila, Philippines in 2014. He is a Professor and Research Faculty at De La Salle University. His main research works include swarm intelligence for underwater swarm robot systems and the development of an underwater swarm robot system.

Argel Bandala completed his doctoral degree in Electronics & Communications Engineering at De La Salle University Manila, Philippines in 2014. He is a Professor and Research Faculty at De La Salle University. His main research work includes the swarming algorithm of unmanned aerial vehicles and artificial intelligence on robotic systems.

Elmer Dadios finished his doctoral degree for an unprecedented two years at Loughborough University (Department of Manufacturing Engineering), United Kingdom in 1996. He is a Full Professor at De La Salle University. His main research interests include artificial intelligence, neural networks, robotics, software engineering, automation, and intelligent systems.

Jonathan Dungca completed his doctoral degree in Civil Engineering at Tokyo Institute of Technology. He is a Full Professor of civil engineering department at De La Salle University Manila, Philippines. His main areas of research are in geotechnical engineering and structural engineering.